Materials and methods

Screening of the sequence variations within the hTERT promoter region. Written informed consent was obtained from all subjects enrolled into the study. Study subjects were genetically unrelated Japanese subjects.

We recruited 46 healthy subjects for screening of polymorphisms within the hTERT promoter region. Among these subjects, the variation(s) in the hTERT sequence (nucleotide number [9] $^{-}$1665 to $^{+}$20) for 17 subjects and the sequence variation at position $^{-}$1327 for 29 subjects were analyzed by a direct DNA sequence analysis.

Luciferase assay. A dual-luciferase reporter assay system (Promega, Madison, WI) was used according to the manufacturer's protocol. A 1.6-kb DNA fragment (nucleotide number [9] $^{-}$1623 to $^{+}$20) with the $^{-1327}$T- or $^{-1327}$C-sequence was subcloned using the TA Cloning Kit (Invitrogen, Carlsbad, CA). Each hTERT insert was subsequently cloned into a firefly luciferase reporter plasmid pGL-3-Basic, a promoter- and enhancer-less vector (Promega), designated pGL3-$^{-1327}$T and pGL3-$^{-1327}$C. Thus, we prepared four types of firefly luciferase reporter plasmids, pGL3-$^{-1327}$T, pGL3-$^{-1327}$C, pGL3-Basic, and pGL3-Control, with the SV40 enhancer/promoter for the normalization of hTERT promoter activity and one *Renilla* luciferase reporter plasmid for standardization of transfection efficiency.

HUVECs (passage number, 3) were purchased from TAKARA (Tokyo, Japan). Early passage HUVECs (passage number, 5–7) were used to avoid the influence of any transformation by subculture on this assay. Transfection with luciferase plasmid into HUVECs was performed using FuGene 6 Transfection Reagent (Roche, Nutley, NJ). Luminescence was measured in each transfectant 24 h and 48 h after transfection. The value corresponding to the transcriptional activity of hTERT promoter for pGL3-$^{-1327}$T or -$^{-1327}$C was calculated using the formula: relative luciferase activity (%) = [(pGL3-$^{-1327}$T or -$^{-1327}$C) − (pGL3-Basic)]/[(pGL3-Control) − (pGL3-Basic)] × 100.

Assay for telomere length. To measure telomere length of leukocyte DNA, as assessed by mean length of terminal restriction fragments (TRF), we used Southern hybridization of telomeric DNA [10] and real-time kinetics quantitative polymerase chain reaction (PCR) [11], and correlation of results by these two methods was previously confirmed [11]. After the confirmation of correlation between these two different methods for measuring telomeres of our samples, we calculated telomere length. Study subjects were 133 males over 40 years of age because the rate of telomere shortening decreases after 40 years of age and is higher in males [12,13]. Genotyping of the $^{-1327}$T/C polymorphism was performed using Megabase 1000 (General Electric, Fairfield, CT), according to the manufacturer's protocol for the single nucleotide primer extension-based method.

Telomerase activity. Telomerase activity in leukocyte from healthy subjects was measured using the method for real-time quantitative PCR telomeric repeat amplification protocol (TRAP) assay, as described previously [14], and telomerase activity in each genotype of the $^{-1327}$T/C polymorphism was analyzed by the values of threshold cycle of telomeric repeat amplification in the real-time quantitative PCR TRAP assay. Nine study subjects were selected to match in age among three genotypes of the $^{-1327}$T/C polymorphism.

Statistics. Mean values of the two groups in this study were compared by Student's t test. Mean values of the three groups in this study were compared by ANOVA. Single regression analysis was used to detect a correlation coefficient (r) in TRF length assay. Statistical analyses were performed using StatView (ver 5.0, for Macintosh, SAS, Cary, NC). A p value less than 0.05 was considered to be statistically significant.

Results

We analyzed the sequence of the hTERT promoter region to screen for genetic variations in 17 subjects, and 2 subjects were showed to be heterozygous for a T to C transition at 1327 bp upstream of the transcription-starting site [9]. This $^{-1327}$T/C transition has been reported (rs 2735940) in the database of single nucleotide polymorphism (http://www.ncbi.nlm.nih.gov/SNP/index.html), although there is no report of epidemiologic or experimental data for this substitution. To examine whether this T/C substitution is polymorphism or not, i.e., this substitution is present more than 1% among population, the genotype distribution of the $^{-1327}$T/C substitution was analyzed in an expanded population of 46 subjects. As a result, the genotype distribution was 15.2% for the $^{-1327}$T/T genotype, 39.0% for the $^{-1327}$T/C genotype, and 45.8% for the $^{-1327}$C/C genotype, suggesting that this T/C substitution is a polymorphism.

To investigate the effects of the $^{-1327}$T/C polymorphism on hTERT transcriptional activity, we performed an experimental study using a dual-luciferase reporter assay system. The mean value of relative luciferase activity representative of hTERT promoter activity in HUVECs transfected with pGL3-$^{-1327}$T was significantly higher than that in HUVECs transfected with pGL3-$^{-1327}$C at 24 h or 48 h after the transfection: 4.592 ± 0.285 (%, mean ± SD) for the pGL3-$^{-1327}$T and 3.711 ± 0.686 for the pGL3-$^{-1327}$C after 24 h of the transfection ($p = 0.0026$), and 6.368 ± 1.017 for the pGL3-$^{-1327}$T and 4.842 ± 0.203 for the pGL3-$^{-1327}$C after 48 h of the transfection ($p = 0.0004$) (data were obtained from three independent experiments performed in triplicate). The results are indicative of the relationship between the $^{-1327}$T-sequence and higher hTERT transcriptional activity.

Next, we measured leukocyte TRF length to test the hypothesis that the $^{-1327}$T/C polymorphism affects telomere length, closely related to the final stages of the telomere system. This speculation was also raised by previous reports that an inter-individual variation in leukocyte telomere length was genetically determined [15,16]. The TRF length in normal leukocytes was significantly different among the three genotypes: 7.80 ± 1.23 (kb, mean ± SD) for the $^{-1327}$C/C genotype ($n = 67$), 8.47 ± 1.04 for the $^{-1327}$T/C genotype ($n = 52$), and 8.53 ± 0.96 for the $^{-1327}$T/T genotype ($n = 14$) ($p = 0.0031$; Fig. 1). When analyzing the telomere length between the subjects without or with the $^{-1327}$T-allele, we obtained the results which showed that the genotypes with $^{-1327}$T/T and $^{-1327}$T/C were significantly longer than that in the $^{-1327}$C/C genotype: 7.80 ± 1.23 (kb, mean ± SD) for the $^{-1327}$C/C genotype ($n = 67$), 8.47 ± 1.04 for the $^{-1327}$T/C and $^{-1327}$T/T genotypes ($n = 66$) ($p = 0.0007$). Mean age was not significantly different between groups: 53.4 ± 5.0 (years, mean ± SD) for the $^{-1327}$C/C, 52.7 ± 4.4 for the $^{-1327}$T/C, and 51.9 ± 4.4 for the $^{-1327}$T/T ($p = 0.5200$). Also, there was no age-related shortening in TRF length in the $^{-1327}$T/T ($r = 0.128$, $p = 0.6633$) and $^{-1327}$T/C subjects ($r = -0.194$, $p = 0.1691$), whereas there was clear age-related telomere shortening in the $^{-1327}$C/C subjects ($r = -0.306$, $p = 0.0117$; Fig. 1). These observations suggest that the $^{-1327}$T/C polymorphism is strongly associated with telomere length in peripheral leukocytes in normal individuals.

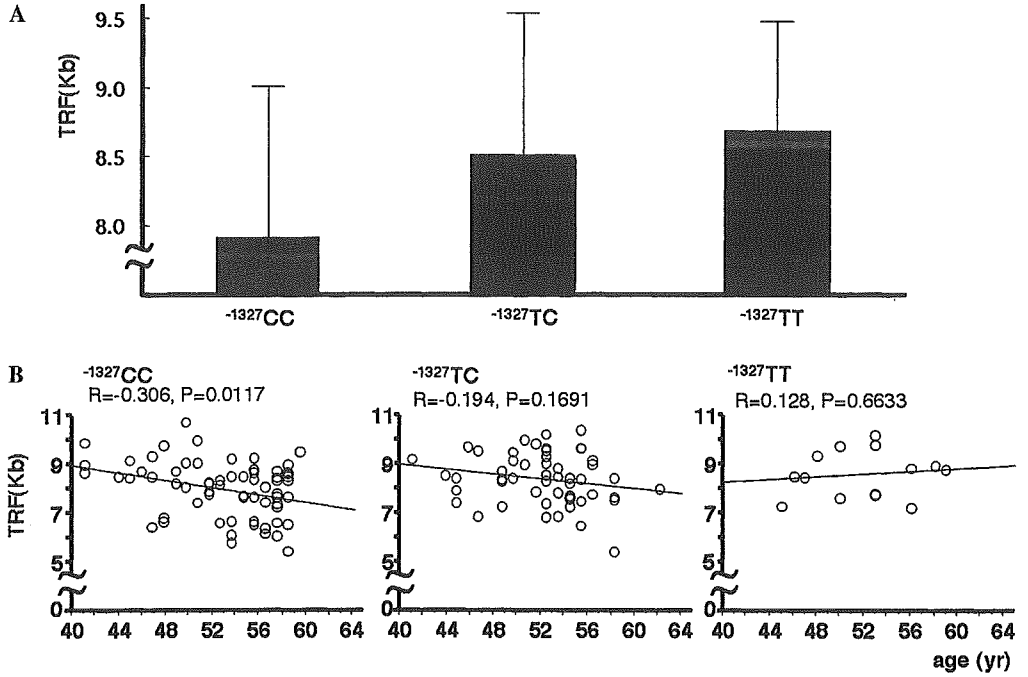

Fig. 1. Relationship between leukocyte telomere length and the $^{-1327}$T/C polymorphism. (A) Bars show mean TRF length (i.e., telomere length) (mean ± SD) in each genotype. (B) Plot of leukocyte TRF length against age and regression line are shown separately for the $^{-1327}$CC, $^{-1327}$TC, and $^{-1327}$TT genotypes.

Telomere length is mainly regulated by telomerase activity that is generally associated with hTERT transcriptional activity. However, several reports showed that transcriptional activity of hTERT did not always correlate directly with telomerase activity and the presence of post-translational modification [17]. Thus, we analyzed the relationship between the $^{-1327}$T/C polymorphism and telomerase activity in leukocyte from healthy subjects, and mean age in each genotype group was 36.0 ± 11.0 (y, mean ± SD) for the $^{-1327}$C/C genotype ($n = 4$), 36.0 ± 7.1 for the $^{-1327}$T/C genotype ($n = 2$), and 36.0 ± 12.2 for the $^{-1327}$T/T genotype ($n = 3$). Telomerase activity was examined using the threshold cycle values (C_t) of telomeric repeat amplification in the real-time quantitative PCR TRAP assay, thus higher C_t indicating lower telomerase activity. Telomerase activity in the subjects with the $^{-1327}$T-allele was higher than that in the subjects without the $^{-1327}$T-allele: 29.9 ± 5.6 (C_t, mean ± SD) for the $^{-1327}$C/C genotype, 28.0 ± 4.2 for the $^{-1327}$T/C genotype, and 21.8 ± 4.0 for the $^{-1327}$T/T genotype, and this difference was marginally significant ($p = 0.0713$). Observation suggests that the $^{-1327}$T-allele is associated with higher telomerase activity in leukocyte.

Discussion

The present study demonstrates for the first time that the $^{-1327}$T/C polymorphism within the hTERT promoter region has functional roles: the $^{-1327}$T sequence is associated with higher transcriptional activity, lack of age-dependent telomere shortening, longer telomere length, and telomerase activity. The relationship of the $^{-1327}$T/C polymorphism to telomere shortening, telomere length, and telomerase activity was found in normal peripheral leukocytes. Leukocyte telomere shortening has been highlighted as a critical marker in the research of cell senescence and cancer, thus, our observations show an impact in the fields.

Transcriptional regulation of hTERT has a key role in telomerase activity and telomere shortening; therefore, we focused on the hTERT promoter region in this study. In our promoter assay, we found approximately a 25% higher promoter activity in the $^{-1327}$T-sequence compared the $^{-1327}$C-sequence. Although the finding with such a modest effect, the data were so strong statistically significant. This significance was caused by the small range of the standard deviations, and possible reasons of the very little inter-assay are as follows; we used a dual-luciferase assay system for standardization of transfection efficiency and early passage HUVECs (passage number, 5–7) to avoid the influence of any transformation by long-term culture on this assay. Particularly, long-term culture of HUVECs showed cell senescence [18]. Although HUVECs have slight activity of telomerase [19], telomerase activity in senescent HUVECs is not fully understood. These suggest that long-term culture of HUVECs is not adapted to evaluate hTERT promoter assay. Thus, we used the present assay system that telomerase promoter with promoter gene works under transient condition using early passage HUVECs although it is important to examine the promoter assay under permanent condition in HUVEC. As a result of careful assay design, we found the relationship of the $^{-1327}$T/C polymorphism on hTERT transcription activity in HUVECs.

We measured leukocyte DNA TRF length, but not that of endothelial cells, because telomere length in both leukocytes and endothelial calls is inversely correlated with age (average decline 30–40 bp/year in normal leukocytes) [12,13,20–22], and leukocyte DNA was available for this study. Also, endothelial cells and leukocytes are exposed to the same hemodynamic stress, thus the rate of turnover is considered to correlate between these cells [21]. The $^{-1327}$T-sequence was strongly associated with longer telomere length. We postulated that $^{-1327}$T-sequence with higher hTERT transcriptional activity is associated with more effective extension of the telomeric end during cell division, and our results reveal a possible causative role of the $^{-1327}$T/C polymorphism in inter-individual variations in leukocyte telomere length.

In conclusion, we report a potential role of the $^{-1327}$T/C polymorphism within the hTERT promoter region in the hTERT promoter activity and leukocyte telomere shortening among normal individuals.

Acknowledgments

We thank Ms. Satomi Tezuka and Ms. Aya Shimizu for their technical support in genetic analysis.

References

[1] G.B. Morin, The human telomere terminal transferase enzyme is a ribonucleoprotein that synthesizes TTAGGG repeats, Cell 59 (1989) 521–529.
[2] A.O. Wilkie, J. Lamb, P.C. Harris, R.D. Finney, D.R. Higgs, A truncated human chromosome 16 associated with alpha thalassaemia is stabilized by addition of telomeric repeat (TTAGGG)n, Nature 346 (1990) 868–871.
[3] J.M. Wong, K. Collins, Telomere maintenance and disease, Lancet 362 (2003) 983–988.
[4] R.M. Cawthon, K.R. Smith, E. O'Brien, A. Sivatchenko, R.A. Kerber, Association between telomere length in blood and mortality in people aged 60 years or older, Lancet 361 (2003) 393–395.
[5] T.M. Nakamura, G.B. Morin, K.B. Chapman, S.L. Weinrich, W.H. Andrews, J. Lingner, C.B. Harley, T.R. Cech, Telomerase catalytic subunit homologs from fission yeast and human, Science 276 (1997) 955–959.
[6] A. Kilian, D.D. Bowtell, H.E. Abud, G.R. Hime, D.J. Venter, P.K. Keese, E.L. Duncan, R.R. Reddel, R.A. Jefferson, Isolation of a candidate human telomerase catalytic subunit gene, which reveals complex splicing patterns in different cell types, Hum. Mol. Genet. 6 (1997) 2011–2019.
[7] A.L. Ducrest, H. Szutorisz, J. Lingner, M. Nabholz, Regulation of the human telomerase reverse transcriptase gene, Oncogene 21 (2002) 541–552.
[8] M. Takakura, S. Kyo, T. Kanaya, H. Hirano, J. Takeda, M. Yutsudo, M. Inoue, Cloning of human telomerase catalytic subunit (hTERT) gene promoter and identification of proximal core promoter sequences essential for transcriptional activation in immortalized and cancer cells, Cancer Res. 59 (1999) 551–557.
[9] I. Horikawa, P.L. Cable, C. Afshari, J.C. Barrett, Cloning and characterization of the promoter region of human telomerase reverse transcriptase gene, Cancer Res. 59 (1999) 826–830.
[10] E. Hiyama, K. Hiyama, T. Yokoyama, T. Ichikawa, Y. Matsuura, Length of telomeric repeats in neuroblastoma: correlation with prognosis and other biological characteristics, Jpn. J. Cancer Res. 83 (1992) 159–164.
[11] R.M. Cawton, Telomere measurement by quantitative PCR, Nucleic Acid Res. 30 (2002) e47.
[12] H. Iwama, K. Ohyashiki, J.H. Ohyashiki, S. Hayashi, N. Yahata, K. Ando, K. Toyama, A. Hoshika, M. Takasaki, M. Mori, J.W. Shay, Telomeric length and telomerase activity vary with age in peripheral blood cells obtained from normal individuals, Hum. Genet. 102 (1998) 397–402.
[13] A. Benetos, K. Okuda, M. Lajemi, M. Kimura, F. Thomas, J. Skurnick, C. Labat, K. Bean, A. Aviv, Telomere length as an indicator of biological aging: the gender effect and relation with pulse pressure and pulse wave velocity, Hypertension 37 (2001) 381–385.
[14] H. Wege, M.S. Chui, H.T. Le, J.M. Tran, M.A. Zern, SYBR green real-time telomeric repeat amplification protocol for the rapid quantification of telomerase activity, Nucleic Acid Res. 31 (2003) e3.
[15] P.E. Slagboom, S. Droog, D.I. Boomsma, Genetic determination of telomere size in humans: a twin study of three age groups, Am. J. Hum. Genet. 55 (1994) 876–882.
[16] B.A. Kosciolek, P.T. Rowley, Human lymphocyte telomerase is genetically regulated, Genes Chromosomes Cancer 21 (1998) 124–130.
[17] Y.H. Hsu, J.J. Lin, Telomere and telomerase as targets for anti-cancer and regeneration therapies, Acta Pharmacol. Sin. 26 (2005) 513–518.
[18] R. Hastings, M. Qureshi, R. Verma, P.S. Lacy, B. Williams, Telomere attrition and accumulation of senescent cells in cultured human endothelial cells, Cell Prolif. 37 (2004) 317–324.
[19] S.M. Bode-Boger, J. Martens-Lobenhoffer, M. Tager, H. Schroder, F. Scalera, Aspirin reduces endothelial cell senescence, Biochem. Biophys. Res. Commun. 334 (2005) 1226–1232.
[20] M. Ogami, Y. Ikura, M. Ohsawa, T. Matsuo, S. Kayo, N. Yoshimi, E. Hai, N. Shirai, S. Ehara, R. Komatsu, T. Naruko, M. Ueda, Telomere shortening in human coronary artery diseases, Arterioscler. Thromb. Vasc. Biol. 24 (2004) 546–550.
[21] E. Chang, C.B. Harley, Telomere length and replicative aging in human vascular tissues, Proc. Natl. Acad. Sci. USA 92 (1995) 11190–11194.
[22] H. Vaziri, F. Schachter, I. Uchida, L. Wei, X. Zhu, R. Effros, D. Cohen, C.B. Harley, Loss of telomeric DNA during aging of normal and trisomy 21 human lymphocytes, Am. J. Hum. Genet. 52 (1993) 661–667.

Journal of Cerebral Blood Flow & Metabolism (2005) 25, 685–693

www.jcbfm.com

Activation of cytokine signaling through leukemia inhibitory factor receptor (LIFR)/gp130 attenuates ischemic brain injury in rats

Shigeaki Suzuki[1], Toru Yamashita[2], Kortaro Tanaka[1], Hidenori Hattori[1], Kazunobu Sawamoto[2], Hideyuki Okano[2] and Norihiro Suzuki[1]

[1]*Department of Neurology, School of Medicine, Keio University, Shinjuku-ku, Tokyo, Japan;* [2]*Department of Physiology, School of Medicine, Keio University, Shinjuku-ku, Tokyo, Japan*

Cytokine signaling through leukemia inhibitory factor receptor (LIFR)/gp130 is known to exert a neurotrophic action in the central nervous system, although the role of this signaling in cerebral ischemia remains unknown. We examined the effect of intracerebral injection of LIF after focal cerebral ischemia in rats. The animals underwent a sham operation (sham group) or middle cerebral artery occlusion (MCAO) followed by direct injection of either vehicle (phosphate-buffered saline, the PBS group) or recombinant LIF (10 ng in the low-LIF group and 100 ng in the high-LIF group) into the cerebral cortex adjacent to the inner boundary zone of the infarct area, and neurologic and histologic evaluations were conducted 24 h later. Expression of LIFR, gp130, and phosphorylated Stat3, Akt, and ERK1/2 was investigated by Western blot analysis and immunohistochemistry. The neurologic deficits and ischemic damage were significantly less severe in the high-LIF group than in the PBS group and the low-LIF group. Leukemia inhibitory factor receptor and gp130 were expressed in neurons, and the ischemic damage of these proteins was rescued in the high-LIF group. Early induction of phosphorylated Stat3 was significantly detected on the ischemic side in the high-LIF group after LIF injection. Exogenous LIF attenuates ischemic brain injury by activating cytokine signaling through LIFR/gp130.
Journal of Cerebral Blood Flow & Metabolism (2005) **25,** 685–693. doi:10.1038/sj.jcbfm.9600061
Published online 16 February 2005

Keywords: gp130; ischemia; leukemia inhibitory factor; neuroprotection; Stat3

Introduction

Leukemia inhibitory factor (LIF) exerts a broad range of effects on many types of cells and has a variety of potential functions in the developing and the mature nervous system (Hilton, 1992). Several *in vitro* studies have clearly shown that LIF promotes differentiation and survival of astrocytes, oligodendrocytes, and specific types of neurons (Guo *et al*, 1999; Nakashima *et al*, 1999), and LIF has also been reported to exert neurotrophic effects in some animal models of central nervous system (CNS) injury such as spinal cord injury, axotomy, and experimental autoimmune encephalomyelitis (EAE) (Tham *et al*, 1997; Blesch *et al*, 1999; Butzkueven *et al*, 2002). Based on these findings, LIF is listed among the growth factors in the CNS (Londreth, 1999).

A common signal transducing receptor component, gp130, acts in association with ligand-specific receptors for members of the interleukin-6 (IL-6) cytokine family, including IL-6, IL-11, LIF, ciliary neurotrophic factor (CNTF), oncostatin-M (OSM), cardiotrophin-1 (CT-1), and cardiotrophin-like cytokine (CLC) (Heinrich *et al*, 2003). Signals induced by LIF, CNTF, OSM, CT-1, and CLC are transduced via a heterodimeric complex of LIF receptor (LIFR) and gp130 (Heinrich *et al*, 2003), but the changes in cellular localization of these receptor components and cytokine signaling through LIFR/gp130 after CNS injury, including cerebral ischemia, have been poorly understood.

Recent studies have demonstrated that expression of LIF and CNTF is upregulated after cerebral ischemia (Suzuki *et al*, 2000; Lin *et al*, 1998), and although CNTF is known to be neuroprotective

Correspondence: Dr S Suzuki, Department of Neurology, School of Medicine, Keio University, 35 Shinanomachi, Shinjuku-ku, Tokyo 160-8582, Japan. E-mail: Shigeaki714@aol.com
This study was supported by grants from the Japanese Ministry of Education, Science, Sports and Culture, and the Keio University Medical Science Fund.
Received 10 August 2004; revised 5 September 2004; accepted 30 September 2004; published online 16 February 2005

against cerebral ischemia (Hermann *et al*, 2001), the role of LIF and cytokine signaling through LIFR/gp130 has remained unexamined. The purpose of the present study was to elucidate the role of cytokine signaling through LIFR/gp130 induced by LIF injection in a rat model of focal cerebral ischemia.

Materials and methods

Animal Preparation

The protocol described here received prior approval from the Committee on Animal Experiment Guidelines of Keio University School of Medicine. Adult male Sprague–Dawley rats (Japan Laboratory Animals, Tokyo, Japan) weighing 270 to 330 g were anesthetized with an intraperitoneal injection of ketamine hydrochloride (100 mg/kg) and xylazine hydrochloride (15 mg/kg). A temperature probe (TD-300; Shibaura Electronics, Tokyo, Japan) was inserted into the rectum, and a heat lamp was used to maintain rectal temperature at 37°C to 37.5°C. Right middle cerebral artery occlusion (MCAO) was induced by the intraluminal filament technique of Belayev *et al* (1996) as previously reported (Suzuki *et al*, 1999). In brief, a 3-0 nylon monofilament suture (Matsuda Ikakogyo, Tokyo, Japan) whose distal segment had been coated with poly-L-lysine solution (Sigma, St Louis, MO, USA) was inserted into the internal carotid artery and advanced until it obstructed the origin of the right MCA. At 30 mins after MCAO, vehicle (0.1 mol/L phosphate-buffered saline (PBS), 10 μL) or recombinant murine LIF (Chemicon, Temecula, CA, USA, 10 ng or 100 ng dissolved in PBS to a total volume of 10 μL) was slowly stereotaxically injected into the cerebral cortex adjacent to the inner boundary zone of the infarct area (0.75 mm posterior to the bregma, 4.0 mm lateral to the midline, and 2.0 mm ventral to the brain surface, Figure 1) (Paxinos and Watson, 1997). The animals were then returned to their cage and given free access to food and water. In the sham operation, a neck incision was made to expose the arteries, but the suture was not inserted into the carotid artery. The other procedures were identical to those described above.

Study Groups

The rats were randomly assigned to 4 groups: a sham group ($n=18$), a PBS group ($n=22$), a low-LIF group ($n=20$), and a high-LIF group ($n=18$). The sham group was subjected to the sham operation followed by PBS injection, and the PBS group was subjected to MCAO followed by PBS injection. The low-LIF and the high-LIF groups were subjected to MCAO followed by a 10 and 100 ng LIF injection, respectively. Animals ($n=54$) were allowed to survive until 24 h after the drug injection. The mortality rate was calculated after excluding deaths caused by anesthesia problems or subarachnoid hemorrhage during the surgical procedures. Before killing, rectal temperature was measured and the animals were examined for neurologic deficits. Remained animals ($n=24$) were killed at 1 or 6 h after the drug injection for experiments of signaling.

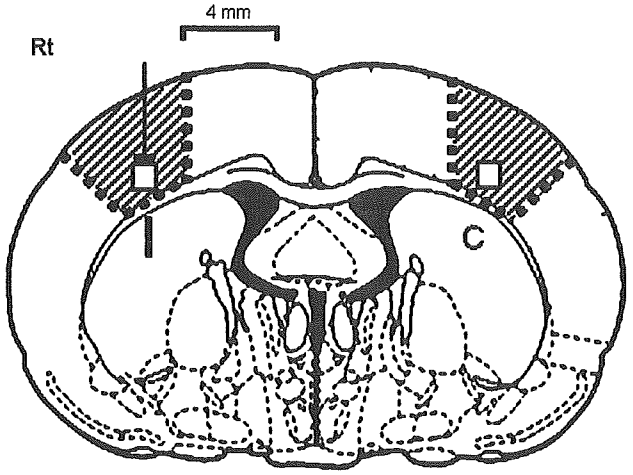

Figure 1 Schematic diagram of the rat coronal brain section (Paxinos and Watson, 1997) at the level of the globus pallidus (0.75 mm posterior to the bregma). The arrow indicates the site of leukemia inhibitory factor (LIF) injection, which corresponded to the region adjacent to the inner boundary zone of the infarct area. Squares indicate the region of interest in which the numbers of TUNEL and immunopositive cells were counted. All photomicrographs presented in Figures 2 and 3 were taken from this square on the ischemic side. Shaded areas indicate the regions from which protein samples were taken for Western blots. I: ischemic side, C: contralateral side.

Neurologic Evaluation

Neurologic deficits were graded as severe, moderate, mild, or absent according to the method devised by Bederson *et al* (1986). In brief, animals that consistently circled were graded as 3. Rats that consistently showed reduced resistance to lateral push toward the left side with no circling movement were graded as 2. Rats with any amount of consistent forelimb flexion but no other abnormalities were graded as 1, and rats with no neurological deficit were graded as 0. Animals were evaluated for neurologic deficits by at least two persons masked to the experimental groups.

Triphenyltetrazolium Chloride Staining

Coronal brain slices were cut at the levels of 0.75 mm posterior to the bregma, and stained with 2% triphenyltetrazolium chloride (TTC) in each groups of animals ($n=3$ or 4 per group).

Infarct Area

At 24 h after the drug injection, animals were perfused with 200 mL of PBS, followed by 200 mL of 4% freshly depolymerized paraformaldehyde in 0.1 mol/L phosphate buffer. The brains were removed and postfixed at 4°C

before cryoprotection by sequential bathing in 10%, 20%, and 30% sucrose. They were then frozen in powdered dry-ice, and consecutive 20-μm thick coronal sections were prepared on a cryostat (Cryocut CM3050S, Leica Instruments GmbH, Nussloch, Germany). Coronal sections prepared from 0.5, 0.75, and 1.0 mm posterior to the bregma were stained with cresyl violet. To quantify the extent of the infarct area in the cerebral cortex, images of the sections were digitized by a computerized digital image analysis system (Inquiry, Loats Associates, Westminister, MD, USA) consisting of a charge-coupled device video camera (CCD72, Dege MTI, Michigan City, IN, USA) with Micro-Nikon lens (Nikon, Tokyo, Japan). An investigator masked to the experimental groups outlined the zone of infarction and the contour of the right and the left hemispheres. The infarct area in the cerebral cortex was calculated by subtracting the area of the normally stained ipsilateral cerebral cortex from the area of the contralateral cerebral cortex to reduce errors because of cerebral edema. The mean values of 3 different sections were reported as a percentage of the entire area of the contralateral cerebral cortex ($n=8$ per group).

TUNEL Staining

Sections were treated with proteinase K, and the fragmented DNA was visualized with biotinylated-dUTP and terminal transferase (TUNEL method) according to the manufacturer's protocol (Roche Diagnostics, Basel, Switzerland). Absolute TUNEL-positive cell counts (per 0.25 mm^2) were made in the regions of interest with an ocular micrometer (Nikon) attached to a light microscope at $\times 200$ magnification, as shown in Figure 1.

Western Blot Analysis

Specimens were collected from the cerebral cortex on both sides as shown in Figure 1. The method used for the Western blot analysis has been described in detail elsewhere (Suzuki *et al*, 1999). In brief, samples containing 20 μg of protein were subjected to 10% polyacrylamide gel electrophoresis. Polyclonal rabbit antibodies for LIFR (1:500 dilution; Santa Cruz Biotechnology, Santa Cruz, CA, USA), gp130 (1:500 dilution; Santa Cruz), phosphorylated Stat3 (Tyr705) (1:250 dilution; Cell Signaling, Beverly, MA, USA), phosphorylated Akt (Ser473) (1:1,000 dilution; Cell Signaling), phosphorylated ERK1/2 (Thr202/Tyr204) (1:1,000 dilution; Cell Signaling), and actin (1:200 dilution; Santa Cruz) were used. Quantitative densitometric analysis of Western blots was performed with a computerized digital image analysis system (Inquiry). The optical density (OD) on the ischemic side was expressed as a percentage of the value on the contralateral side.

Immunohistochemistry

After blocking endogenous peroxidase and nonspecific binding, the sections were incubated overnight at 4°C with rabbit polyclonal anti-LIFR and anti-gp130 antibodies at 1:200 dilution. The slides were then reacted with an avidin-biotinylated enzyme complex system (Vectastain ABC Elite Kit, Vector Laboratories, Burlingame, CA, USA), and the immunoreactive product was visualized with diaminobenzidine (DAB). To assess the specificity of the immunoreactivity, the primary antibody was omitted to provide a nonspecific control. The numbers of LIFR- and gp130-immunoreactive cells were counted as shown in Figure 1. Double-staining immunohistochemistry studies were also performed with the following monoclonal antibodies: anti-NeuN antibody (Chemicon), anti-LIFR antibody (Santa Cruz), anti-GFAP antibody (Boehringer-Mannheim, Philadelphia, PA, USA), anti-adenomatous polyposis coli (APC) antibody (Oncogene, Boston, MA, USA), and isolectin-B4 from *Griffonia simplicifolia* seeds (lectin, Sigma) (Suzuki *et al*, 1999). After incubation with the primary antibodies for 16 h, the sections were incubated for 2 h with a fluorescein isothiocyanate (FITC)-conjugated anti-mouse IgG antibody (Amersham, Buckinghamshire, UK) and a Texas Red-conjugated anti-rabbit IgG antibody (Amersham), and the sections were examined with a fluorescence microscope (Eclipse E-800, Nikon).

Statistical Analysis

All data are reported as means $\pm$ s.d. Neurologic deficits were analyzed with the Mann–Whitney *U*-test. Infarct area, densitometric analysis of Western blots, and cell counts for TUNEL and immunohistochemical staining were analyzed with Student's *t*-test with Bonferroni corrections for multiple simultaneous comparisons. A value of $P<0.05$ was considered statistically significant.

Results

Neurologic Evaluation

The mortality rates, rectal temperatures, and neurologic deficits are summarized in Table 1. All rats in the sham group and the high-LIF group survived until 24 h after the injection, but 25% of the animals in the PBS group and 14% in the low-LIF group died of massive cerebral infarction. Statistic differences on the mortality rate were not obtained. Rectal temperature was lower in the sham group than in the other three groups subjected to MCAO. None of the animals in the sham group exhibited neurologic deficits. The neurologic deficits in the high-LIF group were significantly less severe than in the PBS group ($P=0.02$) and the low-LIF group ($P=0.006$).

Histologic Evaluation

Representative coronal brain slices stained with TTC are shown in Figure 2A. Triphenyltetrazolium chloride staining clearly outlined a massive infarct region in the PBS group and the low-LIF group,

Table 1 Effect of LIF assessed 24 h after the injection

	Sham (n = 12)	*PBS (n = 16)*	*Low-LIF (n = 14)*	*High-LIF (n = 12)*
Mortality rate (%)	0	25	14	0
Rectal temperature (C°)	37.5 ± 0.4[a]	38.1 ± 0.5	38.1 ± 0.5	38.1 ± 0.6
Neurological score (%)[b]				
0 (absent)	100	0	0	0
1 (mild)	0	17	8	58
2 (moderate)	0	17	17	25
3 (severe)	0	66	75	17

[a]Rectal temperature was significantly lower than in the other 3 groups ($P < 0.05$).

[b]The neurological deficits were less severe in the high-LIF group than in the PBS group and the low-LIF group ($P = 0.02$ and 0.006, respectively).

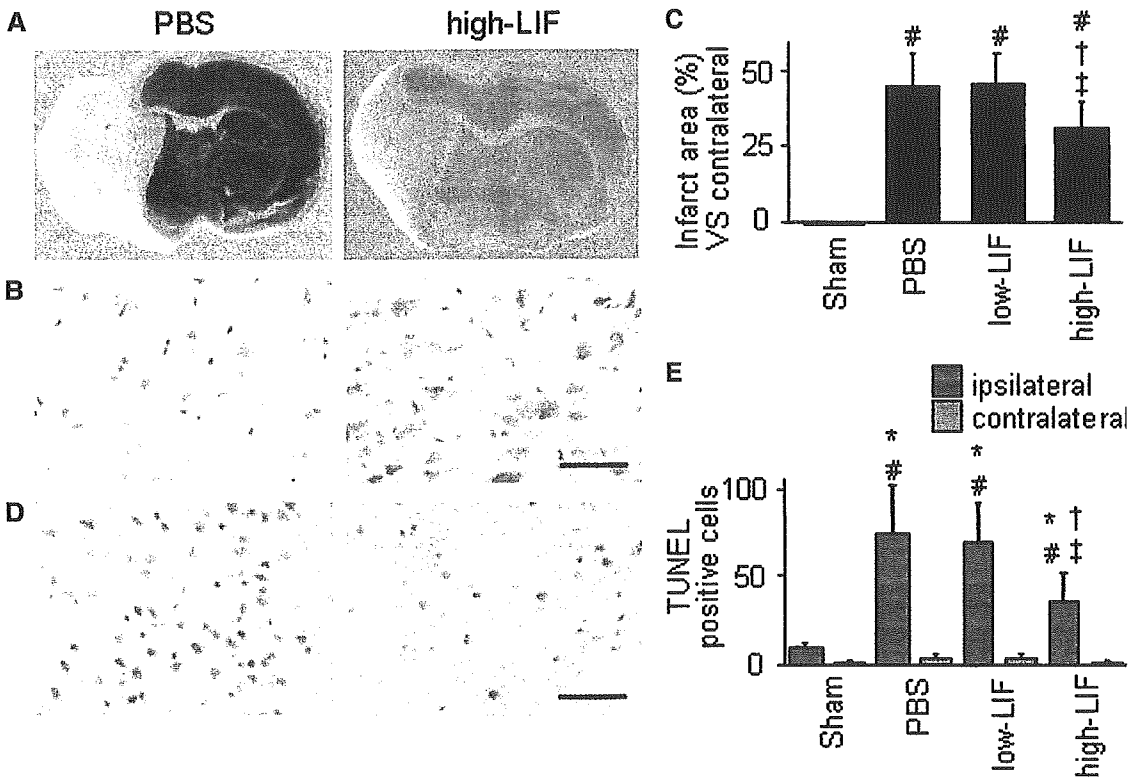

Figure 2 (**A**) Representative photographs showing coronal brain slices with triphenyltetrazolium chloride (TTC) staining in the phosphate-buffered saline (PBS) group and the high-leukemia inhibitory factor (LIF) group. The infarct area (nonstained area) is clearly reduced in the cerebral cortex in the high-LIF group. (**B**) Representative photomicrographs stained with cresyl violet. Ischemic damage is obvious in the PBS group compared with the high-LIF group. (**C**) Infarct area compared with the contralateral cerebral cortex (%) in the 4 groups ($n = 8$ per group). Infarct area was measured on the sections stained with cresyl violet. (**D**) Representative photomicrographs of TUNEL staining. (**E**) Number of TUNEL-positive cells (/0.25 mm^2) in the cerebral cortex on both sides in the 4 groups ($n = 6$ per group). $^*P < 0.05$ versus the contralateral cortex, $^\#P < 0.05$ versus the sham group, $^\dagger P < 0.05$ versus the PBS group, and $^\ddagger P < 0.05$ versus low-LIF group. Bar = 25 μm.

whereas the infarct area in the cerebral cortex was clearly smaller in the high-LIF group. Cresyl violet staining revealed severe ischemic damage in the PBS group and the low-LIF group, while there was less severe in the high-LIF group (Figure 2B). As shown in Figure 2C, the infarct area in the cerebral cortex in the high-LIF group was significantly less than in the PBS group ($P = 0.03$) and the low-LIF group ($P = 0.02$).

The results of TUNEL staining are shown in Figures 2D and 2E. TUNEL-positive cells were detected around the injection site in all groups, but very few TUNEL-positive cells were detected in the contralateral cortex. The number of TUNEL-positive cells on the ischemic side in the high-LIF group were significantly lower than in the PBS group ($P = 0.01$) and the low-LIF group ($P = 0.01$).

Leukemia Inhibitory Factor Receptor and gp130 Expression

The results of the western blot analysis with anti-LIFR and anti-gp130 antibodies are shown in Figures 3A and 3B. Equal expression of LIFR and gp130 protein was detected in the cerebral cortex on both sides in the sham group. Densitometric analysis revealed that expression of both LIFR and gp130 protein on the ischemic side was significantly lower in the PBS group and the low-LIF group than in the sham group. By contrast, expression of both proteins was well preserved in the high-LIF group.

The results of immunohistochemical studies are shown in Figures 3C and 3D. LIFR immunoreactivity was clearly detected in the soma and neurite of the cerebral cortical neurons on both sides in the sham group and on the contralateral side in the

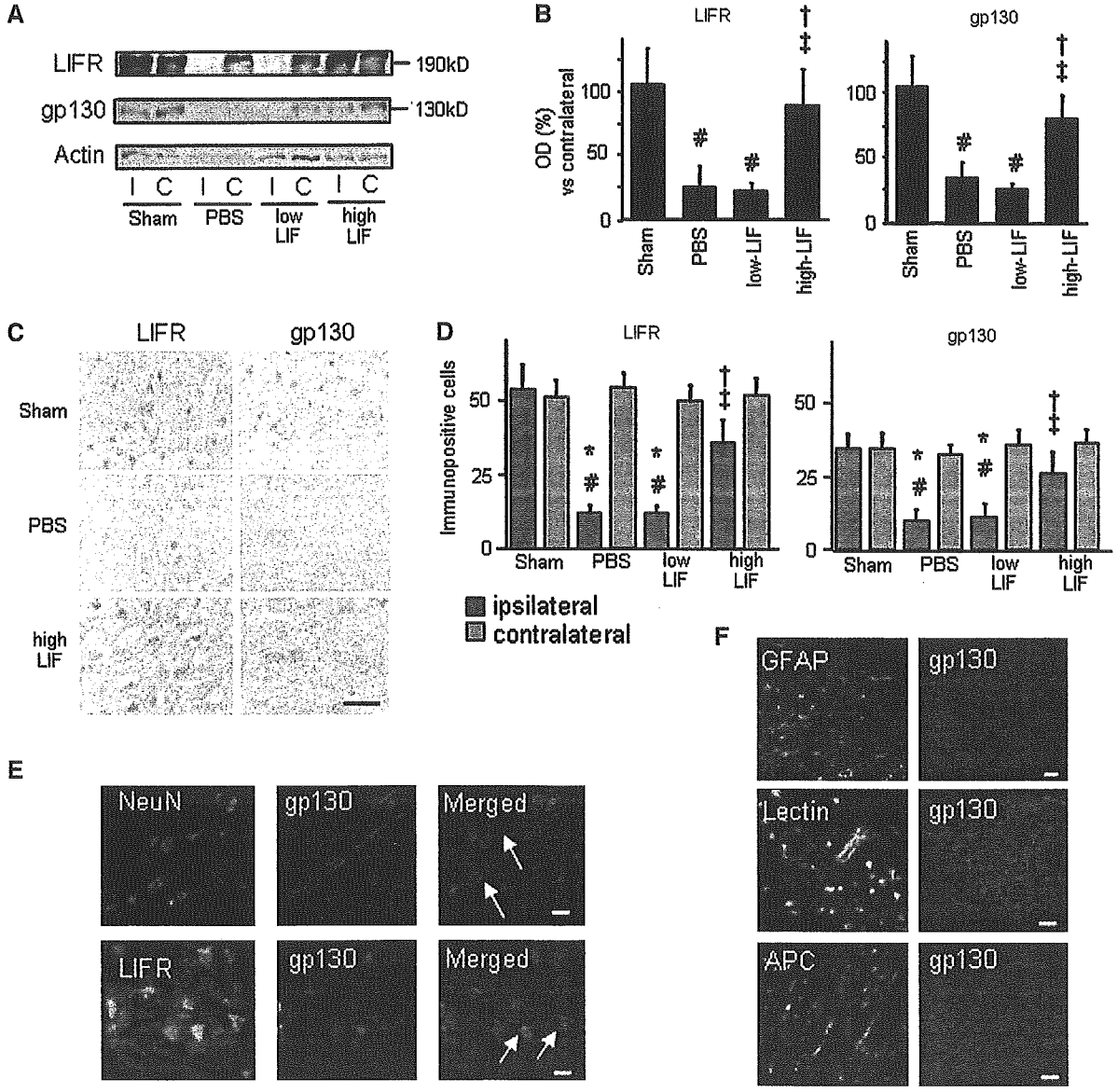

Figure 3 (**A**) Western blot analyses of leukemia inhibitory factor receptor (LIFR), gp130, and actin. Bilateral samples were prepared from the cerebral cortex of the four groups. I: ischemic side, C: contralateral side. (**B**) Optical density (OD) of each protein band on the ischemic side expressed as percentage of the OD on the contralateral side ($n = 4$ per group) (**C**) Representative photomicrographs showing immunoreactivity with anti-LIFR and anti-gp130 antibodies on the ischemic side. LIFR- and gp130-immunoreactivity was markedly decreased in the phosphate-buffered saline (PBS) group, but well preserved in the high-LIF group. (**D**) Numbers of LIFR- and gp130-immunopositive cells (/0.25 mm^2) in the cortex on both sides in the 4 groups ($n = 6$ per group). (**E**) NeuN/gp130 and LIFR/gp130 double-staining immunohistochemistry. gp130-immunoreactivity was colocalized with NeuN and LIFR (arrows). (**F**) GFAP/gp130, Lectin/gp130, and APC/gp130 double-staining immunohistochemistry. The distribution of glial cells was different from that of gp130 expression. $^*P < 0.05$ versus the contralateral cortex, $^\#P < 0.05$ versus the sham group, $^\dagger P < 0.05$ versus the PBS group, and $^\ddagger P < 0.05$ versus low-LIF group. I: ischemic side, C: contralateral side. Bar = 25 μm.

other three groups. Immunoreactivity for gp130, however, was localized in the soma of neurons. There were fewer LIFR- and gp130-immunopositive neurons on the ischemic side in the PBS group and the low-LIF group, and these findings were consistent with the Western blot data. The numbers of LIFR- and gp130-immunopositive cells on the ischemic side were significantly higher in the high-LIF group than in the PBS group and the low-LIF group. No immunoreactivity was detected when the primary antibodies were omitted. Double-staining immunohistochemistry showed that the gp130-immunopositive cells were exclusively neurons (Figure 3E) and that some neurons expressed both LIFR and gp130 (Figure 3E). Glial cells, including astrocytes, microglia, and oligodendrocytes, had proliferated in the ischemic region at 24 h after the injection, but the distribution of the glial cells was different from that of the LIFR- and gp130-immunopositive cells (Figure 3F). These findings indicate that the main source of LIFR and gp130 was neurons.

Phosphorylation of Stat3, Akt, and Erk1/2

The temporal profile of the Western blot analyses showed that Stat3, Akt, and Erk1/2 were phosphorylated at 1 h after the drug injection (Figure 4A). Densitometric analysis revealed that early induction of phosphorylated Stat3 was significantly detected on the ischemic side in the high-LIF group at 1 and 6 h after LIF injection (Figure 4B). Although the phosphorylation of Akt and Erk1/2 was induced after cerebral ischemia, densitometric analysis revealed that an increase in phosphorylation of these proteins in the high-LIF group at 1 and 6 h after LIF injection was small and not statistically significant compared with the PBS group and the low-LIF group.

Discussion

We selected the region adjacent to the inner boundary zone of the infarct area as the site of LIF injection for the following reasons. First, we had already showed that endogenous LIF is expressed in the cerebral cortical neurons in the peri-ischemia area, and its expression peaked at 24 h after MCAO (Suzuki *et al*, 2000). By contrast, expression of endogenous LIF was suppressed in the region adjacent to the inner boundary zone of infarct area. Second, this region corresponds to the ischemic penumbra that can be salvaged by pharmacological agents (Memezawa *et al*, 1992).

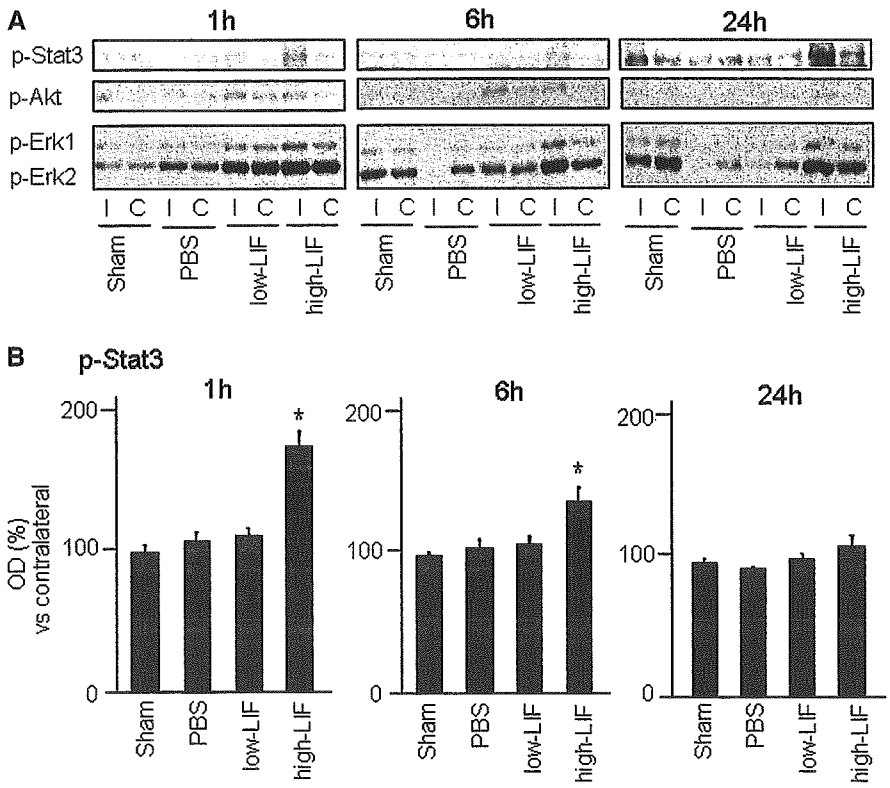

Figure 4 (**A**) Temporal profile of the Western blot analyses findings for phosphorylated Stat3, Akt, and Erk1/2. Samples were prepared from the cerebral cortex on both sides in the 4 groups at 1, 6, and 24 h after the injection. I: ischemic side, C: contralateral side. (**B**) Optical density (OD) of phosphorylated Stat3 on the ischemic side expressed as percentage of the OD on the contralateral side ($n = 3$ or 4 per group). *$P < 0.05$ versus the other 3 groups.

Leukemia inhibitory factor receptor and gp130 have been shown to be located in the cerebral and cerebellar neurons in normal rat brain (Watanabe *et al*, 1996; Yamakuni *et al*, 1996; Morikawa *et al*, 2000), although the alterations in these receptor components under pathological conditions was varied by investigators (Haas *et al*, 1999; Getchell *et al*, 2002; Choi *et al*, 2003). Getchell *et al* (2002) reported upregulation of LIFR mRNA in the olfactory receptor neurons after olfactory bulb ablation. Haas *et al* (1999) found that gp130 mRNA levels were unaltered in the rat facial nucleus after axotomy, but Choi *et al* (2003) reported that gp130 mRNA was upregulated after cerebral ischemia. Leukemia inhibitory factor receptor has also been reported to be increased in the spinal cord in EAE, but gp130 is not increased (Butzkueven *et al*, 2002). Taken together, we concluded that the alterations in these receptor components depended on the model of the CNS injury. In the clinical study, it was reported that the serum concentration of soluble gp130 was significantly reduced the first week after stroke (Acalovschi *et al*, 2003). We showed that the main source of LIFR and gp130 under both normal and ischemic conditions is neuron, and that the loss of these proteins was rescued by LIF injection.

Much attention had been paid to the role of LIFR/gp130 in the developing and mature CNS, and cytokine signaling through LIFR/gp130 has been reported to be necessary for the maintenance of forebrain neuronal stem cells and the survival of postmitotic neurons during development (Shimazaki *et al*, 2001). Leukemia inhibitory factor receptor/gp130 signaling also reduced immune-mediated demyelination by enhancing oligodendrocyte survival (Butzkueven *et al*, 2002), and either LIFR- or gp130-deficient mice exhibited significant loss of motor neurons (Nakashima *et al*, 1999; Li *et al*, 1995). Based on these findings, we speculated that the LIFR/gp130-mediated signaling induced by LIF injection had a significant neuroprotective effect on the cerebral ischemia in the present study.

We propose the presumed downstream signal pathways through LIFR/gp130, which are activated by LIF (Figure 5). It is now acceptable that these signaling pathways are closely associated with the cell survival and anti-apoptosis (Alonzi *et al*, 2001; Park *et al*, 2003; Heinrich *et al*, 2003). Among them, JAK-STAT is the most important pathway, and is strongly regulated by Tyr705 phosphorylation of Stat3 (Heinrich *et al*, 2003). In the present study, we demonstrated that recombinant LIF induced especially Stat3 phosphorylation, and the JAK-STAT was the main pathway activated after cerebral ischemia. In addition, PI3K/Akt and MEK/Erk1/2 pathways are also known to be activated after LIF injection (Alonzi *et al*, 2001; Park *et al*, 2003), but their activation was less than that of JAK-STAT.

Although we and other investigators have reported enhanced phosphorylation of Stat3 after cerebral ischemia (Justicia *et al*, 2000; Suzuki *et al*, 2001; Wen *et al*, 2001), the exact role of Stat3 phosphorylation has not been elucidated. Wen *et al* (2001) observed that phosphorylated Stat3-positive neurons were also TUNEL-positive and speculated that this signal plays a crucial role in ischemia-induced neuron death. By contrast, we found that LIF injection induced rapid enhancement of Stat3 phosphorylation, indicating that LIF may be associated with an important neuroprotective role against cerebral ischemia. In this regard, we had already shown that Stat3 phosphorylation is predominantly detected in surviving neurons after transient MCAO (Suzuki *et al*, 2001). In addition, IL-6 was proven to have neuroprotective effects against cerebral ischemia (Loddick *et al*, 1998; Herrmann *et al*, 2003). We recently found that the administration of anti-IL-6 receptor antibody to mice after MCAO enlarged the infarct size and aggravated the neurological deficits together with a significant reduction in Stat3 phosphorylation (Yamashita *et al*, submitted). Based on these findings, we concluded that Stat3 phosphorylation after cerebral ischemia was closely related to neuroprotection. Because we demonstrated that LIF could decrease the number of TUNEL-positive cells, the most important neuroprotective mechanism of Stat3 phosphorylation was antiapoptosis. In fact, it was reported that the role of Stat3 on cell survival has been linked to the transcriptional regulation of apoptotic regulatory proteins such as Bcl-2 family (Battle and Frank, 2002).

The present study showed that proliferating glial cells, including astrocytes, microglia, and

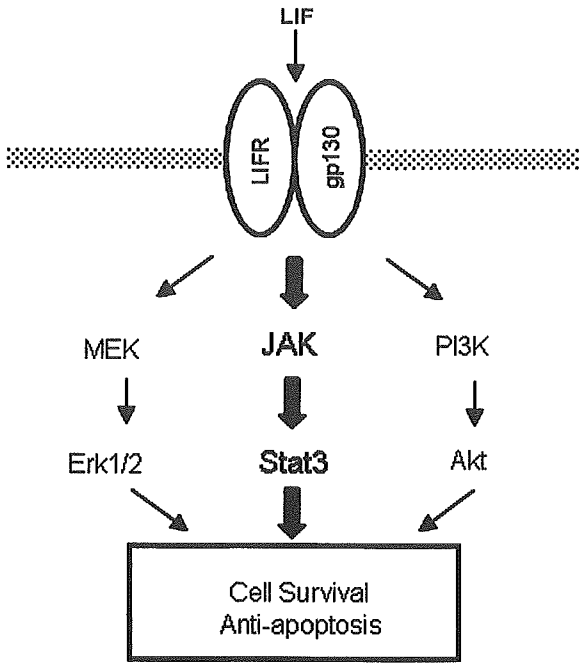

Figure 5 A presumed diagram of signaling pathways through Leukemia inhibitory factor receptor/gp130, which are activated by leukemia inhibitory factor (LIF).

oligodendroglia, are not the main source of LIFR and gp130. One of the reasons why gp130 was not detected in glial cells may be because of the sensitivity of polyclonal antibody used in this study. Unfortunately, it was an only commercially available antibody for immunohistochemistry. The survival and differentiation of astrocytes and oligodendroglia have been shown to be potentiated by LIFR/gp130 signaling, and astrocyte differentiation is dramatically impaired in either gp130- or LIFR-deficient mice (Nakashima *et al*, 1999; Butzkueven *et al*, 2002). In fact, activation of the JAK-STAT pathway involving Stat3 was observed in reactive astrocytes after cerebral ischemia (Choi *et al*, 2003; Justicia *et al*, 2000), and we have showed expression of endogenous LIF in astrocytes at 96 h of reperfusion after transient MCAO (Suzuki *et al*, 2000). Taken together, we think that an experimental protocol with a longer period after cerebral ischemia will be necessary to determine the exact role of signaling through LIFR/gp130 in glial cells.

In summary, we have demonstrated that recombinant LIF can attenuate ischemic brain injury in rats by activating cytokine signaling through LIFR/gp130.

References

Acalovschi D, Wiest T, Hartmann M, Farahmi M, Mansmann U, Auffarth GU, Grau AJ, Green FR, Grond-Ginsbach C, Schwaninger M (2003) Multiple levels of regulation of the interleukin-6 system in stroke. *Stroke* 34:1864–70

Alonzi T, Middleton G, Wyatt S, Buchman V, Betz UAK, Müller W, Musiani P, Poli V, Davies AM (2001) Role of STAT3 and PI 3-kinase/Akt in mediating the survival actions of cytokines on sensory neurons. *Mol Cell Neurosci* 18:270–82

Battle TE, Frank DA (2002) The role of STATs in apoptosis. *Curr Mol Med* 2:381–92

Bederson JB, Pitts LH, Tsuji M, Nishimura MC, Davis RL, Bartkowski H (1986) Rat middle cerebral artery occlusion: evaluation of the model and development of a neurologic examination. *Stroke* 17:472–6

Belayev L, Alonso OF, Busto R, Zhoa W, Ginsberg MD (1996) Middle cerebral artery occlusion in the rat by intraluminal suture, neurological and pathological evaluation of an improved model. *Stroke* 27:1616–23

Blesch A, Uy HS, Grill RJ, Cheng JG, Patterson PH, Tuszynski MH (1999) Leukemia inhibitory factor augments neurotrophin expression and corticospinal axon growth after adult CNS injury. *J Neurosci* 19:3556–66

Butzkueven H, Zhang JG, Soilu-Hanninen M, Hochrein H, Chionh F, Shipham KA, Emery B, Turnley AM, Petratos S, Ernst M, Bartlett PF, Kilpatrick TJ (2002) LIF receptor signaling limits immune-mediated demyelination by enhancing oligodendrocyte survival. *Nat Med* 8:613–9

Choi JS, Kim SY, Cha JH, Choi YS, Sung KW, Oh ST, Kim ON, Chung JW, Chun MH, Lee SB, Lee MY (2003) Upregulation of gp130 and STAT3 activation in the rat hippocampus following transient forebrain ischemia. *Glia* 41:237–46

Getchell TV, Shah DS, Partin JV, Subhedar NK, Getchell ML (2002) Leukemia inhibitory factor mRNA expression is upregulated in macrophages and olfactory receptor neurons after target ablation. *J Neurosci Res* 67:246–54

Guo X, Chandrasekaren V, Lein P, Kaplan PL, Higgins D (1999) Leukemia inhibitory factor and cilliary neurotrophic factor cause dendritic retraction in cultured rat sympathetic neurons. *J Neurosci* 19:2113–21

Haas CA, Hofmann HD, Kirsch M (1999) Expression of CNTF/LIF-receptor components and activation of STAT3 signaling in axotomized facial motoneurons: evidence for a sequential postlesional function of the cytokines. *J Neurobiol* 41:559–71

Heinrich PC, Behrmann I, Haan S, Hermanns HM, Muller-Newen G, Schaper F (2003) Principles of interleukin (IL)-6-type cytokine signalling and its regulation. *Biochem J* 374:1–20

Hermann DM, Kilic E, Kugler S, Isenmann S, Bahn M (2001) Adenovirus-mediated GDNF and CNTF pretreatment protects against striatal injury following transient middle cerebral artery occlusion in mice. *Neurobiol Dis* 8:655–66

Herrmann O, Tarabin V, Suzuki S, Attigah N, Coserea I, Schneider A, Vogel J, Prinz S, Schwab S, Monyer H, Brombacher F, Schwaninger M (2003) Regulation of body temperature and neuroprotection by endogeneous interleukin-6 in cerebral ischemia. *J Cereb Blood Flow Metab* 23:406–15

Hilton DJ (1992) LIF: lots of interesting functions. *Trends Biochem Sci* 17:72–6

Justicia C, Gabriel C, Planas AM (2000) Activation of the JAK/STAT pathway following transient focal cerebral ischemia: signaling through Jak1 and Stat3 in astrocytes. *Glia* 30:253–70

Li M, Sendtner M, Smith A (1995) Essential function of LIF receptor in motor neurons. *Nature* 378:724–7

Lin TN, Wang PY, Chi SI, Kuo JS (1998) Differential regulation of ciliary neurotrophic factor (CNTF) and CNTF receptor α (CNTFα) expression following focal cerebral ischemia. *Mol Brain Res* 55:71–80

Loddick SA, Turnbull AV, Rothwell NJ (1998) Cerebral interleukin-6 is neuroprotective during permanent focal cerebral ischemia in the rat. *J Cereb Blood Flow Metab* 18:176–9

Londreth GE (1999) Growth factors. In: *Basic neurochemistry* (Siegel GJ, eds), Philadelphia: Lippincott-Raven, 383–98

Memezawa H, Smith ML, Siesjo BK (1992) Penumbral tissues salvaged by reperfusion following middle cerebral artery occlusion in rats. *Stroke* 23:552–9

Morikawa Y, Tohya K, Tamura S, Ichihara M, Miyajima A, Senba E (2000) Expression of interleukin-6 receptor, leukemia inhibitory factor receptor and glycoprotein 130 in the murine cerebellum and neuropathological effect of leukemia inhibitory factor on cerebellar Purkinje cells. *Neuroscience* 100:841–8

Nakashima K, Wiese S, Yanagisawa M, Arakawa H, Kimura N, Hisatsune T, Yoshida K, Kishimoto T, Sendtner M, Taga T (1999) Developmental requirement of gp130 signaling in neuronal survival and astrocyte differentiation. *J Neurosci* 19:5429–34

Park JI, Strock CJ, Ball DW, Nelkin BD (2003) The Ras/Raf/MEK/extracellular signal-regulated kinase pathway induces autocrine-paracrine growth inhibition via the leukemia inhibitory factor/JAK/STAT pathway. *Mol Cell Biol* 23:543–54

Paxinos G, Watson C (1997) *The rat brain in stereotaxic coordinates. Compact 3rd edn.* San Diego: Academic Press

Shimazaki T, Shingo T, Weiss S (2001) The ciliary neurotrophic factor/leukemia inhibitory factor/gp130 receptor complex operates in the maintenance of mammalian forebrain neural stem cells. *J Neurosci* 21:7642–53

Suzuki S, Tanaka K, Nogawa S, Nagata E, Ito D, Dembo T, Fukuuchi Y (1999) Temporal profile and cellular localization of interleukin-6 protein after focal cerebral ischemia in rats. *J Cereb Blood Flow Metab* 19:1256–62

Suzuki S, Tanaka K, Nogawa S, Ito D, Dembo T, Kosakai A, Fukuuchi Y (2000) Immunohistochemical detection of leukemia inhibitory factor after focal cerebral ischemia in rats. *J Cereb Blood Flow Metab* 20:661–8

Suzuki S, Tanaka K, Nogawa S, Dembo T, Kosakai A, Fukuuchi Y (2001) Phosphorylation of signal transducer and activator of transcription-3 (Stat3) after focal cerebral ischemia in rats. *Exp Neurol* 170:63–71

Tham S, Dowsing B, Finkelstein D, Donato R, Cheema SS, Bartlett PF, Morrison WA (1997) Leukemia inhibitory factor enhances the regeneration of transected rat sciatic nerve and the function of reinnervated muscle. *J Neurosci Res* 47:208–15

Watanabe D, Yoshimura R, Khalil M, Yoshida K, Kishimoto T, Taga T, Kiyama H (1996) Characteristic localization of gp130 (the signal-transducing receptor component used in common for IL-6/IL-11/CNTF/LIF/OSM) in the rat brain. *Eur J Neurosci* 8:1630–40

Wen TC, Peng H, Hata R, Desaki J, Sakanaka M (2001) Induction of phosphorylated-Stat3 following focal cerebral ischemia in mice. *Neurosci Lett* 303:153–6

Yamakuni H, Minami M, Satoh M (1996) Localization of mRNA for leukemia inhibitory factor receptor in the adult rat brain. *J Neuroimmunol* 70:189–98

Journal of Cerebral Blood Flow & Metabolism (2005) 25, 742–747

www.jcbfm.com

Initial oligemia with capillary flow stop followed by hyperemia during K^+-induced cortical spreading depression in rats

Minoru Tomita[1], Istvan Schiszler[1], Yutaka Tomita[2], Norio Tanahashi[1], Hidetaka Takeda[1], Takashi Osada[1] and Norihiro Suzuki[1]

[1]*Department of Neurology, School of Medicine, Keio University, Tokyo, Japan;* [2]*Laboratoire de Biologie et Physiologie Moléculaire du Vaisseau, Paris, France*

Local cerebral blood volume (CBV) and capillary flow changes in regions of depolarizing neurons during K^+-induced cortical spreading depression (CSD) in the cerebral cortex of α-chloralose-urethane-anesthetized rats were examined employing a transillumination (550 nm) video system. Capillary flow was calculated as the reciprocal of mean transit times of blood in pixels of 40 μm × 40 μm, each of which contains a few capillaries. Potassium microinjection into the cortex evoked repetitive wave-ring spreads of oligemia at a speed of ca. 2.33 ± 0.48 mm/min. During the spread of CSD, tracer (either saline or carbon black) was injected into the internal carotid artery. Colocated with the oligemic wave, we detected capillary flow stop as evidenced by disappearance of the hemodilution curves. At any location in the region of interest within the cerebral cortex, we observed cyclic changes of capillary flow stop/hyperperfusion in synchrony with oligemia/hyperemia fluctuations. The initial flow stop and oligemia were ascribed to capillary compression by astroglial cell swelling, presumably at the pericapillary endfeet, since the oligemia occurred before larger vessel changes. We conclude that local depolarizing neurons can decrease adjacent capillary flow directly and immediately, most likely via astroglial cell swelling, and that the flow stop triggers upstream arteriolar dilatation for capillary hyperperfusion.
Journal of Cerebral Blood Flow & Metabolism (2005) **25,** 742–747. doi:10.1038/sj.jcbfm.9600074
Published online 23 February 2005

Keywords: astroglial swelling; blood transit; hemodilution curve; light transmission image through the cortex; neurovascular coupling; wave-ring spread of oligemia

Introduction

The relationship between neuronal functional changes and blood flow changes, and the mechanisms involved, remains unknown (Tomita *et al*, 2002). Cortical spreading depression (CSD) could provide a good experimental model to examine the relationship between neuronal depolarization and flow changes. Although there have been abundant reports on vascular changes and flow changes during CSD in the literature (Back *et al*, 1994; Dreier *et al*, 2001; Duckrow, 1993; Dunn *et al*, 2001; Fabricius *et al*, 1995; Hansen and Lauritzen, 1984; Leão and Morrison, 1945; Marshall, 1959; Nielsen *et al*, 2000; Van Harreveld and Stamm, 1952), the findings were rather inconsistent, especially with respect to early local flow changes.

This communication describes a comprehensive examination of capillary flow changes in the cerebral cortex during K^+-induced CSD (neuronal depolarization) by employing a new optical method with a high spatial resolution which has recently been developed by us (Schiszler *et al*, 2000).

Correspondence: Dr Minoru Tomita, Department of Neurology, School of Medicine, Keio University, 35 Shinanomachi, Shinjuku-ku, Tokyo 160-8582, Japan. E-mail: mtomita@sc.itc.keio.ac.jp
This study was supported by a research grant from the New Energy and Industrial Technology Development Organization, and funds from the Mihara Award received by M.T. for his stroke research activity in 2001.
Received 7 June 2004; revised 30 September 2004; accepted 21 October 2004; published online 23 February 2005

Materials and methods

Experiments were performed on 10 Sprague–Dawley rats under α-chloralose-urethane anesthesia. The optical method employed here was as reported elsewhere (Schiszler *et al*, 2000). A transillumination technique was applied, despite possible damage arising from optical fiber insertion into the brain tissue, because any changes in the light

transmission (LT) at $\lambda = 550 \pm 10$ nm, one of the isosbestic points of hemoglobin, are attributable to changes in cerebral blood volume (CBV) (Tomita M *et al*, 1978). Images of the brain surface in a 2 mm × 2 mm region of interest (ROI) were focused with a Nikon lens and monitored with a silicon intensified target (SIT) camera (Hamamatsu Photonics, Hamamatsu, Japan). The transilluminated cortical images were continuously recorded on videotape at 30 frames/s (30 Hz) or fed into a personal computer through a Scion LG-3 frame grabber card (Scion Corporation, MD, USA) with 512^2 pixels at various acquisition rates (0.5 to 15 Hz). The acquired images in the Scion frame grabber card were automatically scaled logarithmically in topographical brightness to 8-bit images, and displayed as pictures on the 256 gray scale. Frame-by-frame subtraction between two pictures at 0.5-sec intervals was performed to visualize clearly the wave-ring image because of the CBV changes and arteriolar diametric changes during CSD.

After a 1-h period to allow for recovery from the stress of optical-fiber insertion, K^+ solution (a few μL, 500 mmol/L) was microinjected at a depth of ca. 1 mm into the cortical parenchyma at the center of the ROI through a glass micropipette (originally constructed for intracellular injection). During continuous video-recording of the ROI after CSD induction, 25 μL of saline (a negative blood indicator) in 6 rats and diluted carbon black solution in 2 rats was injected as a spike into the internal carotid artery via a catheter inserted into the external carotid artery. The principle and assumptions underlying the measurements of flow in a 'pixel' (100 averaged Scion pixels) were as follows. A pixel of 40 μm × 40 μm should contain only a few capillaries, since average intercapillary distance is 22 μm when calculated from the rat cortical microvasculature moulded in a Mercox cast (MT, unpublished observation). The mean transit time (MTT) calculated from the hemodilution curve represents the reciprocal velocity of blood passing through the capillaries in the pixel. The hemodilution curves for all the individual pixels of a 50 × 50 matrix in the ROI were analyzed with Matlab software (The MathWorks, Inc., Natick, USA) to evaluate the MTTs by employing a customized algorithm of the area/height of hemodilution curves ($\mathrm{MTT} = \int t\,\Delta\mathrm{LT}(t)\,dt / \int \Delta\mathrm{LT}(t)\,dt$, where ΔLT is the light transmission change in a pixel). The reciprocal mean transit time (1/MTT) was taken to represent the capillary flow (either transit of red blood cells (RBC) when saline is used or plasma transit when carbon black is used), which was arranged in appropriate coordinates to construct a two-dimensional (2-D) flow map with the aid of our own software, KEIO-IS1. The 2-D flow map so constructed had a resolution of 625 flow values/mm^2, which is ca. 500-fold higher spatial resolution than that of conventional laser-Doppler flowmetry. We noticed that near-zero flow values thus calculated were either incorrectly estimated by the software, which automatically included small baseline fluctuations into the height for MTT calculation, or were uncalculated because zero was divided by zero ($0(t\,\Delta\mathrm{LT}(t))/0(\Delta\mathrm{LT}(t))$) with no build-up of hemodilution curve. In the latter case, the capillary flow must be 0, whereas the computer automatically yielded a certain value based on noise. To avoid further artificial error, no correction was made to the values in Table 1.

Table 1 Parameters in early flow changes

Parameters	*v (mm/s)*	$T_{1/2}$ *(s)*	T_k *(1/s)*	T_i *(s)*	$Flow_i$ *(%)*	$Flow_h$ *(%)*
Rat 1	3.2	0.75	0.94	9.5	5	160
Rat 2	2.5	0.88	0.78	8.2	60	240
Rat 3	2.2	1.09	0.64	7.5	5	200
Rat 4	1.8	1.07	0.65	4.2	60	250
Rat 5	2.1	0.46	1.51	6.8	20	210
Rat 6	2.2	2.11	0.33	8.1	40	230
Mean	2.33	1.06	0.81	7.4	31.6*	215.0*
±s.d.	0.48	0.56	0.40	1.8	25.4	32.7

v = speed of CSD, $T_{1/2}$ = the half-decrease time of capillary flow decrease, T_k = the time constant, T_i = oligemic period, $Flow_i$ = the lowest flow, and $Flow_h$ = the highest flow in the hyperemic period. *Changes were statistically significant ($P < 0.05$) when compared to control values.

Rapid changes in capillary flow at the very beginning of neuronal depolarization were examined as follows. Since a 2-D map during CSD depicts a series of changes from 'no flow' to subsequent hyperperfusion in a panoramic view, a plot profile of capillary flow changes along a line passing through the injection site could broadly be concomitant with CSD propagation towards the periphery. The conversion of the distance/time scale was made by using the speed of individual CSDs in mm/sec (CSD velocity (v)). Thus, determined parameters were the time constant of initial flow decrease (T_k in 1/s) calculated from the half-decrease time ($T_{1/2}$ in secs) assuming an exponential decay, the oligemic duration (T_i in secs), the relative change in low flow level (F_i in %), and the subsequent hyperemic level (F_h in %). These changes were examined for statistical significance using the nonparametric Wilcoxon signed rank test. No correction was made for overestimation of F_i due to baseline noise as mentioned above.

Results

General Description of Cortical Spreading Depression

As described in our previous report (Tomita Y *et al*, 2002), K^+ injection into the cerebral cortex produced, after a latency of several minutes, a concentric light wave-ring spread as shown in subtraction pictures (Figures 1A to 1C). The K^+ injection immediately created a dark spot of ca. 100 μm in diameter, which was hardly visible to the naked eye, at the site of injection. The spot changed its shape polymorphically with time and sometimes seemed to be 'boiling'. After a period of several seconds to a couple of minutes, a corona-like white projection at the edge of the dark spot started to appear and fused into a concentric ring of increased LT. As shown, the ring gradually increased in diameter, propagating peripherally, like the ripples evoked by a stone dropped into a pond. This was

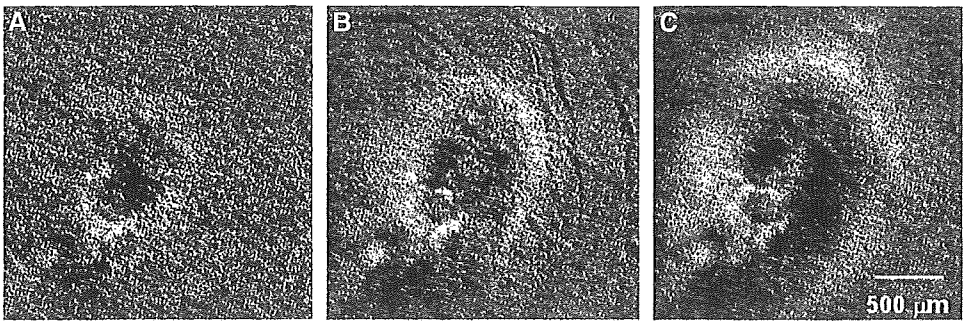

Figure 1 Frame-by-frame subtraction pictures at intervals of 0.5 sec to show wave-ring spread of light transparency (a decrease of CBV) at a speed of 3 mm/min. Vascular diametric changes of small vessels are seen at 8 secs after CSD induction.

followed by a wide dark band, forming an expanding doughnut shape. The presence of pial vessels did not influence the wave-ring propagation. A few minutes after the first sequence, a second sequence of wave-ring spreading from the same 'boiling' center started. The individual expanding concentric rings were slightly different in width and darkness, but the expansion was concentric with respect to the area stimulated by K^+ injection. The dynamic wave-ring spread was repeated at intervals of 2 to 5 mins for more than 30 mins in 3 rats. The spread speed was 2.33 ± 0.48 mm/min (mean $\pm$ s.d.). Since the cortex was transilluminated by light at a wavelength of 550 nm, the spreading light ring was considered to be due to a blood volume decrease (oligemia), followed by a wide, dark band of blood volume increase (hyperemia). Approximately >5 secs after the CSD induction, there appeared thread-like structures of presumably arteriolar diametric changes (constriction or dilatation) during a period within the 0.5-sec frame interval, as seen in the frame-by-frame subtraction picture B of Figure 1. It should be noted that the arteriolar changes occurred after, not before, the tissue oligemia had started. In three other rats, the spread was abortive: the dark band appeared, but gradually subsided, and finally disappeared. We failed to produce CSD in two rats because of bleeding and inappropriate K^+ injection, and to measure MTT in two rats because of failure of catheter insertion into the external carotid artery.

During passage of the wave-ring spread, no bulge or dent of the brain surface was observed by employing reflected light.

Capillary Flow Changes with Cortical Spreading Depression

Saline injection into the internal carotid artery yielded 2500 hemodilution curves in the ROI of the rat brain. All hemodilution curves are included in Figure 2, where continuous LT traces (the intensities of the transmitted light through the cortical tissue layer) were recorded from 2500 pixels during the first CSD spread. There were five arrays

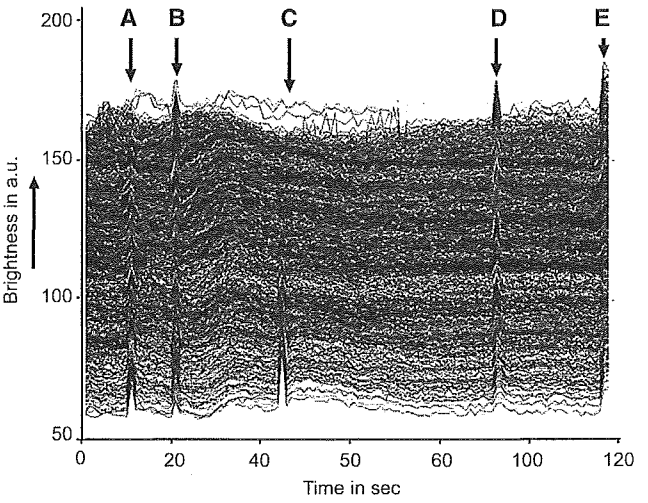

Figure 2 Records of 2500 LT traces at pixels containing a few capillaries in the cerebral cortex for 120 secs. Upward direction is brighter. Baselines fluctuate because of irregular RBC transits. Note that hemodilution curve buildups are not uniform, depending on oligemic wave passage. Intracarotid saline injections were made five times at (**A**)–(**E**). Capillary flow stop is indicated by the absence of hemodilution curves in the upper part at the first (**A**) and third (**C**) injections, but reappeared at the second (**B**), fourth (**D**), and fifth (**E**) injections.

of sharp waves (hemodilution curves A, B, C, D, and E) induced by the saline injections. The height of the curves reflects the amount of saline and therefore the blood distributed to the area at that moment (Tomita M *et al*, 1983). The distribution displayed a tremendous variability at different locations and different moments during the CSD spread, contrasting with the rather even distribution under control conditions. At the time points indicated by arrows A and C in Figure 2, the upper part of the traces reveals no buildup of hemodilution curves, implying that blood was not supplied to the area where the light wave with CSD was just passing. This implies that capillary perfusion was halted in the area at that moment. However, at the following moments, for example, at times B, D, and E, the same area began to

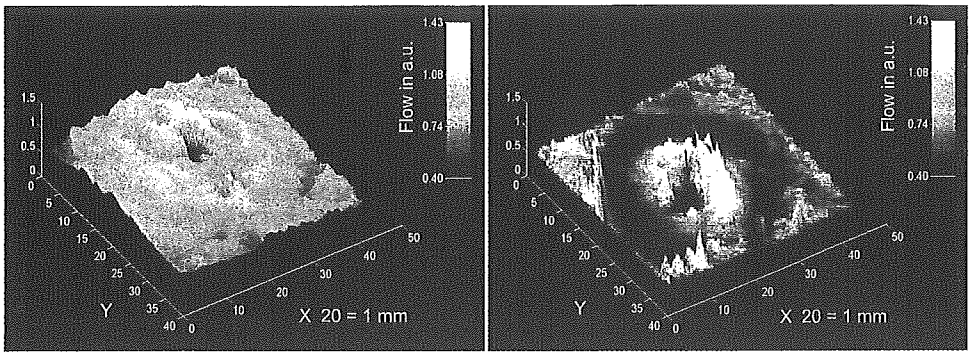

Figure 3 Three-dimensional capillary flow maps in the ROI reconstructed from 2500 capillary flow values (reciprocal MTTs) which were calculated from hemodilution curves after intracarotid saline injection (left) and diluted carbon black injection (right) during CSD. Note the wave-ring shape of capillary flow changes. The ordinate is blood flow in arbitrary units (a.u.). Note that flows obtained from carbon black dilution curves are lower than those from saline because of the slowness of plasma (carbon black) transit compared with RBC (saline; negative indicator of RBC) transit, resulting in a lower tissue hematocrit of ca. 66%.

receive blood supply. Such on-and-off tidal capillary flow changes with CSD in time and space were seen at any spot in the surrounding cerebral cortex. The appearance of hemodilution curves and the level of the baseline brightness were fairly well correlated, except for a certain refractory period. Figure 3 (left) depicts the 2-D capillary flow map, where the wavefront of a low flow ring showing a decrease is mostly colocated at the light ring area of oligemia. The low flow band was followed by a high flow band with a more than two-fold increase in capillary flow with high CBV. Figure 3 (right) shows a 2-D capillary flow map based on carbon black dye dilution curves, which exhibits more clearly a low-flow (dark) ring followed by a high-flow (hyperemic) band. The average flow values in Figure 3 (right) were lower than those of Figure 3 (left) due to the low tissue hematocrit (flow values obtained by using carbon black (plasma indicator) were ca. 66% lower than those obtained by saline (RBC (negative) indicator) (Tomita and Gotoh, 1982).

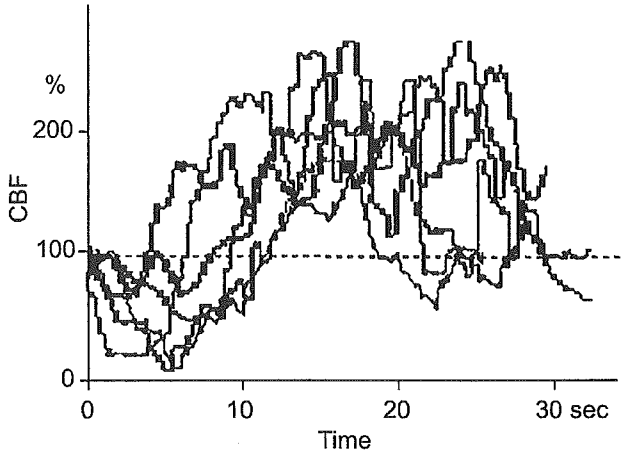

Figure 4 Capillary flow changes on a horizontal line passing through the site of K^+-injection are shown. As can be seen, an initial decrease in capillary flow occurred in all six cases ($P<0.05$), followed by marked hyperperfusion ($P<0.05$).

Plot Profile of Capillary Flow and Other Parameters

Plot profiles of capillary flow varied greatly, not only with 2-D capillary flow maps obtained successively in the same rat, but even with line angles in the same flow map. Figure 4 represents the plot profile (time courses) of capillary flow along a line passing through the injection site obtained from six cases studied with saline injection. Calculated parameters are presented in Table 1. As shown, capillary flow immediately decreased in all six cases ($P<0.05$). The average change was from the control (100%) to $31.6\% \pm 25.4\%$. Subsequently, capillary flow increased markedly in all six cases ($P<0.05$) to $215.0\% \pm 32.7\%$. If we consider the fact that no dilution curves built up at the lowest point, the flow values must have reached practically 0% (flow stop), even though the computer yielded higher values.

Discussion

The essential point of this paper is to show the presence of a moving wave-ring of initial transient oligemic and low (or no) flow in the cerebral cortex during CSD. These oligemic rings appeared to be independent of the locations of arterial arborization or microcirculatory units. Such rapid initial capillary flow changes might have been overlooked in the literature because of the poor spatial resolution of the conventional methods so far employed to study flow. For example, the most commonly used laser Doppler flowmeter, having a probe of 1 mm in diameter, measures only average flow values within the sensitive surface area (one-quarter of the 2-D capillary flow map shown in Figure 3). The laser Doppler flowmeter would miss the subtle local flow changes that we observed, owing to averaging within the area, yielding a variety of changes

depending on the location of the probe: an increase, a decrease, or even no change (Tomita M *et al*, 2001). One may consider that the capillary flow stop could be secondary to upstream arteriolar constriction, as suggested by van Harreveld and Ochs (1957). However, contrary to their proposal of vascular origin, we consider that the oligemic changes were neuronal in origin for the following reasons. (1) Arteriolar changes occurred >5 secs after the onset of tissue oligemia (Figure 1B); (2) the speed of flow decrease to capillary flow stop (time constant of 0.81/s) could not be explained by the upstream arteriolar constriction; (3) the ring distribution of oligemia cannot be explained by arteriolar flow supply; and (4) the oligemic area is narrower than the reported size (500 μm in diameter) of the microcirculatory unit. According to our experience, capillary flow does not stop immediately after arterial occlusion, presumably due to residual vasomotion in the microvascular network. The vasomotion (to-and-fro movements) of RBC in capillaries would persist at least for 20 secs. Our data suggest the change in capillary flow is more directly associated with neuronal inactivation. Among many possibilities, capillary flow redistribution in the microvascular network would occur from time to time due to partial capillary flow resistance changes. We speculate that resistance of individual capillaries in the oligemic region is increased by astroglial swelling coupled with neuronal depolarization. In particular, the pericapillary endfeet processes of astroglial cells would swell and compress embracing capillaries rapidly. Newman (1986) reported that a large fraction of the total cell conductance of astroglial cells for ions is localized at the endfeet processes. This may assist rapid perivascular astroglial swelling. Van Harreveld and Schade (1959) noted that sodium and chloride ions moved from the intercellular space to cellular components during CSD. Van Harreveld (1958) recognized a 30% swelling of apical dendrites of glial cells during CSD. The cell swelling was reported to be explosive when conditions were appropriate, as seen in heart muscle cells (Kloner *et al*, 1974), as well as in brain cells (Hossmann, 1971) under conditions of severe membrane depolarization and sufficient environmental fluid. Mori *et al* (2002) recently confirmed that the extracellular space started to decrease at 34 secs after global ischemia and reached half-maximum change at 123 secs. The immediate water shift is due to anomalous osmosis, involving the movement of water into cells coupled with the flow of sodium ions across the cell membrane (Nagasawa *et al*, 1986; Tomita and Gotoh, 1992; Tomita, 2005, in press). The rapid CBV decrease with ischemia may occur reciprocally with astroglial swelling. When a middle cerebral artery was occluded in cats, we observed a rapid CBV decrease from 6.3 to 5.2 vol% at 20 secs after the occlusion (Tomita *et al*, 1980), a time which coincides with the time of EEG disappearance (neuronal depolarization). If the astroglial-swelling scenario is correct, the resultant 'cuff' compression of capillaries by swollen astroglial endfeet could be so rapid that RBC flow through the capillaries would be virtually halted. The slightest decrease of the capillary lumen would be sufficient to increase flow resistance steeply owing to the inverse Fåhraeus Lindqvist effect (Chien, 1972). Flowing RBC would start to escape the resistant channels toward nearby less-resistant channels in the capillary networks. This might be called a kind of 'steal' event from capillaries with higher resistance to surrounding capillaries with lower resistance. Nevertheless, the possibilities of direct contraction of vascular endothelial cells constituting capillaries (Inoue *et al*, 2003) in response to a rapid signal from depolarizing neurons, and hemorheological events of 'plasma skimming' at capillary branches remain to be excluded.

After the oligemic period of approximately 5 to 8 secs, the local tissue underwent hyperemia and hyperperfusion due to arteriolar dilatation, in agreement with previous reports. Many regulatory mechanisms due to arteriolar responses to tissue oligemia through multimodal feedback routes would begin to operate at this point.

Acknowledgements

We thank Professor William I Rosenblum and Professor Konstantin-Alexander Hossmann for their critical reading of the manuscript and helpful suggestions.

References

Back T, Kohno K, Hossmann KA (1994) Cortical negative DC deflections following middle cerebral artery occlusion and KCl-induced spreading depression: effect on blood flow, tissue oxygenation, and electroencephalogram. *J Cereb Blood Flow Metab* 14:12–9

Chien S (1972) Present state of blood rheology. In: *Hemodilution* (Messmer K, Schmid-Schonbein H, eds), Basel: Karger S, 1–45

Dreier JP, Petzold G, Tille K, Lindauer U, Arnold G, Heinemann U, Einhäupl KM, Dirnagl U (2001) Ischaemia triggered by spreading neuronal activation is inhibited by vasodilators in rats. *J Physiol* 531:515–26

Duckrow RB (1993) A brief hypoperfusion precedes spreading depression if nitric oxide synthesis is inhibited. *Brain Res* 618:190–5

Dunn AK, Bolay H, Moskowitz MA, Boas DA (2001) Dynamic imaging of cerebral blood flow using laser speckle. *J Cereb Blood Flow Metab* 21:195–201

Fabricius M, Akgoren N, Lauritzen M (1995) Arginine–nitric oxide pathway and cerebrovascular regulation in cortical spreading depression. *Am J Physiol* 269:H23–H9

Hansen AJ, Lauritzen M (1984) The role of spreading depression in acute brain disorders. *Ann Acad Bras Cienc* 56:457–79

Hossmann K-A (1971) Cortical steady potential, impedance and excitability changes during and after total ischemia of cat brain. *Exp Neurol* 32:163–75

Inoue K, Tomita M, Fukuuchi Y, Tanahashi T, Kobari M, Takao M, Takeda H, Yokoyama M (2003) Dynamic observation of oxygenation-induced contraction of and transient fiber-network formation/disassembly in cultured human brain microvascular endothelial cells. *J Cereb Blood Flow Metab* 23:821–8

Kloner RA, Ganote CE, Whalen DA, Jennings RB (1974) Effect of a transient period of ischemia on myocardial cells: II. Fine structure during the first few minutes of reflow. *Am J Pathol* 74:399–422

Leão AAP, Morrison RS (1945) Proportion of spreading cortical depression. *J Neurophysiol* 8:33–45

Marshall WH (1959) Spreading cortical depression of Leão. *Physiol Rev* 39:239–79

Mori K, Miyazaki M, Iwase H, Maeda M (2002) Temporal profile of changes in brain tissue extracellular space and extracellular ion (Na(+), K(+)) concentrations after cerebral ischemia and the effects of mild cerebral hypothermia. *J Neurotrauma* 19:1261–70

Nagasawa M, Tasaka M, Tomita M (1986) Coupled transport of water and ions through membranes as a possible cause of cytotoxic edema. *Neurosci Lett* 66: 19–24

Newman EA (1986) High potassium conductance in astrocyte endfeet. *Science* 233:453–4

Nielsen AN, Fabricius M, Lauritzen M (2000) Scanning laser-Doppler flowmetry of rat cerebral circulation during cortical spreading depression. *J Vasc Res* 37:513–22

Schiszler I, Tomita M, Fukuuchi Y, Tanahashi N, Inoue K (2000) New optical method for analyzing cortical blood flow heterogeneity in small animals: validation of the method. *Am J Physiol* 279:H1291–H8

Tomita M (2005) Increased intracranial pressure and brain edema. In: *Pathology & genetics. Cerebrovascular diseases* (Kalimo H, ed), Basel, Switzerland: ISN Neuropath Press, in press

Tomita M, Fukuuchi Y, Tanahashi N, Kobari M, Tomita Y, Ohtomo M (2001) Heterogeneity of 'microflow' changes within a cortical area as small as an LDF probe [abstract]. *J Cereb Blood Flow Metab* 21(Suppl 1):S228

Tomita M, Gotoh F (1982) Which circulates faster through the cerebral microcirculatory system, red cells or plasma? *Stroke* 13:722

Tomita M, Gotoh F, Amano T, Tanahashi N, Kobari M, Shinohara T, Mihara B (1983) Transfer function through regional cerebral cortex evaluated by a photoelectric method. *Am J Physiol* 245:H385–H98

Tomita M, Gotoh F (1992) Cascade of cell swelling (cytotoxic edema): thermodynamic potential discharge of brain cells following membrane injury. *Am J Physiol* 262:H603–H10

Tomita M, Gotoh F, Amano T, Tanahashi N, Tanaka K (1980) 'Low perfusion hyperemia' following middle cerebral arterial occlusion in cats of different age groups. *Stroke* 11:629–36

Tomita M, Gotoh F, Sato T, Amano T, Tanahashi N, Tanaka K, Yamamoto M (1978) Photoelectric method for estimating hemodynamic changes in regional cerebral tissue. *Am J Physiol* 235:H56–H63

Tomita M, Kanno K, Hamel E (2002) *Brain activation and CBF control, International Congress Series 1235.* Amsterdam: Elsevier Science, BV

Tomita Y, Tomita M, Schiszler I, Amano T, Tanahashi N, Kobari M, Takeda H, Ohtomo M, Fukuuchi Y (2002) Repetitive concentric wave-ring spread of oligemia/hyperemia in the sensorimotor cortex accompanying K^+-induced spreading depression in rats and cats. *Neurosci Lett* 322:157–60

Van Harreveld A. (1958) Changes in the diameter of apical dendrites during spreading depression. *Am J Physiol* 192:457–63

Van Harreveld A, Ochs S (1957) Electrial and vascular concomitants of spreading depression. *Am J Physiol* 189:156–66

Van Harreveld A, Schade JP (1959) Chloride movements in cerebral cortex after circulatory arrest and during spreading depression. *J Cell Comp Physiol* 54:65–84

Van Harreveld A, Stamm JS (1952) Vascular concomitants of spreading cortical depression. *J Neurophysiol* 15:487–96